

Detection of symmetry-protected topological phases in one dimension with multiscale entanglement renormalization

Hsueh-Wen Chang(張學文),¹ Yun-Da Hsieh (謝昀達),¹ and Ying-Jer Kao (高英哲)^{1,2}

¹*Center for Theoretical Science and Department of Physics, National Taiwan University, Taipei 106, Taiwan*

²*Center for Advanced Study in Theoretical Science, National Taiwan University, Taipei 10607, Taiwan*

(Dated: October 17, 2018)

Symmetry-protected topological (SPT) phases are short-range entangled quantum phases with symmetry, which have gapped excitations in the bulk and gapless modes at the edge. In this paper, we study the SPT phases in the spin-1 Heisenberg chain with a single-ion anisotropy D , which has a quantum phase transition between a Haldane phase and a large- D phase. Using symmetric multiscale entanglement renormalization ansatz (MERA) tensor networks, we study the nonlocal order parameters for time-reversal and inversion symmetry. For the inversion symmetric MERA, we propose a brick-and-rope representation that gives a geometrical interpretation of inversion symmetric tensors. Finally, we study the symmetric renormalization group (RG) flow of the inversion symmetric string-order parameter, and show that entanglement renormalization with symmetric tensors produces proper behavior of the RG fixed-points.

PACS numbers: 02.70.-c, 75.10.Pq, 05.10.Cc

I. INTRODUCTION

Phases of matter are traditionally characterized by local order parameters associated with spontaneous symmetry breaking. This is the essence of the Landau paradigm of phase transitions. However, there are states of matter which fall beyond this type of characterization. One famous example is the fractional quantum Hall state, which is topologically ordered with no local order parameter.¹ Topological phases are often characterized by a gapped ground state in the bulk and the presence of gapless edge modes.² Classification of these topological phases remains difficult since there is no-symmetry breaking associated with these phases. Using the ideas based on local unitary transformations, it is argued that an *intrinsic* topological order is associated with the pattern of long-range entanglements in gapped quantum systems with finite topological entanglement entropy.³

The situation in one dimension(1D) is quite different. The *intrinsic* topological order as described above exists only in two and higher dimensions since the ground states of all one-dimensional gapped spin systems are in a single phase.⁴ However, if we impose symmetries on the system, there might exist topological phases which are protected by the presence of the symmetry. These symmetry-protected topological (SPT) phases are formed by gapped short-range-entangled quantum states that do not break any symmetries.⁵ The Haldane phase of odd-integer spin chains⁶ is an example of a SPT phase in one dimension.^{5,7} In addition, by tuning some parameters in the Hamiltonian, it is possible to drive a quantum phase transition between two topologically inequivalent phases through a critical point. Classification of these SPT phases is not easy since there exists no spontaneous symmetry breaking, i.e., no local order parameters, on both sides of the critical point. It is desirable to find some quantities that change through the critical point to characterize the phase transition.⁷

One representative example of the Haldane phase is the spin-1 AKLT state, which is the ground state of an exact solvable AKLT model.⁸ The AKLT state exhibits no conventional

long-range order, but can be characterized by nonlocal string-order and edge states.^{9,10} By measuring a string of identical operators with distinct end points, it can be shown the system exhibits correlations that are independent of the string length, indicating a string-order in the system. Later, it is realized that the string-order parameter can be generalized to distinguish different SPT phases, if symmetry operations on the entanglement between blocks is considered.^{3,7} Studying the symmetry operation on the matrix product state (MPS), nonlocal string-order parameters have been constructed to characterize SPT states for different types of global symmetries.^{11–13} In this work, we demonstrate how to use a symmetry-protected multiscale entanglement renormalization ansatz (MERA)^{14,15} to calculate string-order parameters in the presence of time-reversal and inversion symmetry for a spin-1 chain.

MERA is a real-space renormalization group (RG) method based on the concept of entanglement renormalization.^{16,17} By inserting disentanglers into the system to remove short-range entanglement before renormalization, it prevents the accumulation of degrees of freedom during the real-space RG transformation. This method have been applied to several 1D and 2D systems,^{17–20} and even at quantum critical points.²¹ MERA with a global Z_2 symmetry, which the time-reversal symmetry belongs to, has been proposed for the case of parity.²² On the other hand, the algorithm for constructing an inversion-symmetric MERA is not yet available in the literature.²³ Examining the coarse-graining process of MERA and the relation between the geometrical inversion and the tensor symmetry, we construct an inversion symmetric MERA based on a “brick-and-rope” representation. This enables us to study the inversion symmetric string-order parameter using inversion symmetric MERA.

This paper is structured as follows: We first introduce the spin-1 chain model and review some of its properties in Sec. II. In Sec. III, we discuss how to implement a Z_2 symmetric MERA and introduce our algorithm on inversion symmetric MERA based on a brick-and-rope representation. In Sec. IV, we present the results of string-order parameters using both time-reversal and inversion symmetric MERA. We

conclude our work in Sec. VI.

II. MODEL

We study the spin-1 Heisenberg model with a single-ion anisotropy term on a periodic chain of length N :

$$H = \sum_{i=1}^N \mathbf{S}_i \cdot \mathbf{S}_{i+1} + D \sum_{i=1}^N (S_i^z)^2. \quad (1)$$

For $D \rightarrow 0$, the ground state is in the Haldane phase, which is topologically non-trivial.⁵ The AKLT state, which is exact solvable, is known to describe the same phase as the Haldane phase.⁸ For $D \gg 1$, the ground state is in the large- D phase,⁵ which is topologically equivalent to the product state $|0\rangle^{\otimes N}$ in the S_z basis and is a topologically trivial state. By tuning D , there is a Gaussian transition from the Haldane phase to the large- D phase near $D_c = 0.96845(8)$.²⁴ This model has translation, spatial inversion, time-reversal symmetries, and a $Z_2 \times Z_2$ symmetry of rotations $\mathcal{R}_x = \exp(i\pi S^x)$ and $\mathcal{R}_z = \exp(i\pi S^z)$.^{9,10} For the purpose of this paper, we will focus on inversion and TR symmetries, while the translation symmetry is considered explicitly in the MERA tensor network.

III. SYMMETRIES IN MULTISCALE-ENTANGLEMENT RENORMALIZATION ANSATZ

In this section, we will briefly review the algorithms for MERA, and discuss how to incorporate the time-reversal (Z_2) symmetry.^{17,22} Finally, we will give a detailed description of an implementation for the inversion symmetry.

A. Multiscale-Entanglement Renormalization Ansatz

Figure 1 shows an example of a 1D ternary (three-to-one) MERA network. The fundamental tensors in the structure are the disentangler (u), and the isometry (w). From a RG transformation perspective, an isometry coarse-grains, in this case, three sites into one effective site. A disentangler u acts across the boundary of two blocks of sites to remove short-range entanglement between the blocks.^{16,17} The u 's and w 's satisfy the unitarity constraints (Fig. 1):

$$u^\dagger u = uu^\dagger = \mathbb{I}^{\otimes 2} \quad (2)$$

$$w^\dagger w = \mathbb{I} \quad (3)$$

An important implication of these constraints is that the tensor contraction process can be simplified and only tensors inside a “causal cone” structure need to be contracted (shaded area in Fig. 2). To facilitate our discussion on symmetry operations in the following, we will interpret u as a transformation of the incoming wave function in the *original* basis, while w corresponds to a transformation to a *truncated* basis with χ basis states.

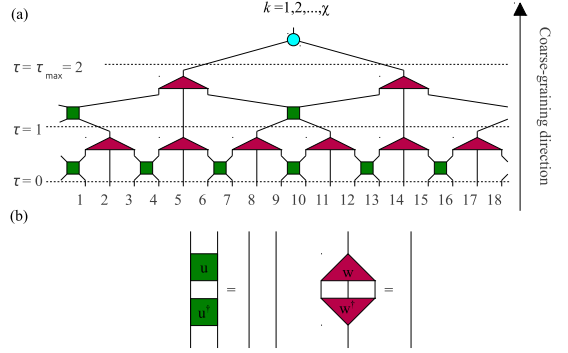


FIG. 1. (Color online) (a) The structure of an 18-site 1D ternary MERA with the periodic boundary condition. In addition to the (horizontal) physical direction, there is also a (vertical) coarse-graining direction. While coarse-graining, we truncate the less important degree of freedom by w . At the top layer, a reduced basis of χ states is kept and we find the minimum energy state inside this truncated Hilbert space. (b) Diagrammatic representation of the isometric constraints for the disentanglers u and the isometries w .

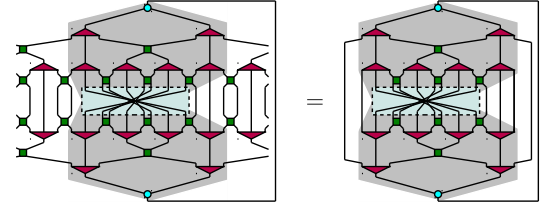


FIG. 2. (Color online) Diagram of an inversion symmetric string-order parameter of eight inverted sites in MERA. Shaded area corresponds to the causal cone in which the tensor contraction needs to be performed. The width of the causal cone grows with the size of the swapped region.

Since our model is translationally invariant, we set the disentanglers and isometries in each layer identical. In the simulation, we initiate the tensors obeying the constraints Eqs. (2) and (3), and perform updates respecting these conditions. We treat the tensor coefficients as variational parameters, and optimize u 's and w 's by minimizing the energy.¹⁷ We perform updates on u or w by a singular value decomposition (SVD) of the environment tensor for the given tensor. We refer interested readers to Ref. 17 for details of this procedure. Figure 2 shows a typical calculation of the inversion symmetric string-order parameter. The width of the causal cone scales with the number of the inverted sites, which must be contained in the causal cone at the physical layer. To simplify the contraction, we want to use symmetric tensors to remove these symmetry-related operators.

B. Z_2 symmetric MERA

Several important symmetry operations, such as time-reversal (TR) and parity fall into a general class of an internal

Z_2 symmetry. In the following, we will use the TR symmetry for spin-1 as a concrete example to discuss the algorithm, and it can be easily generalized to any internal Z_2 symmetries.²²

Define the global TR symmetry operator $O \equiv (O_T)^{\otimes N}$, where O_T is the TR symmetry operator acting on each bond with $O_T^2 = 1$. To represent a symmetric state, we use a MERA composed of symmetric tensors,¹⁴ where the symmetric isometry, w , and disentangler, u , satisfy

$$(O_T \otimes O_T)u^\tau(O_T^\dagger \otimes O_T^\dagger) = u^\tau \quad (4)$$

$$(O_T)w^\tau(O_T^\dagger \otimes O_T^\dagger \otimes O_T^\dagger) = w^\tau \quad (5)$$

With these conditions, the TR symmetry is preserved during the RG transformation and the Hamiltonian at the τ -th layer, H^τ , is also TR symmetric. We obtain the ground state in a specific symmetry sector by diagonalizing the top Hamiltonian $H^{\tau_{\max}}$. The top density matrix is also TR symmetric and the symmetry is also preserved as we descend down to the physical layer. Treating the u and w tensors as linear operators, the MERA network, denoted by \mathcal{M} , can be regarded as a collection of operators with internal bonds contracted. Therefore, a TR symmetric MERA should also satisfy the operator identity

$$[\mathcal{M}, O] = 0. \quad (6)$$

Graphically, Eq. 6 can be represented by Figs. (3a) and (e). Since the TR symmetry is an internal symmetry, we can decompose the global operator O into local symmetry operators O_T as in Fig. (3b). If each tensor commutes with the local TR operator O_T , we can *lift* the TR operators layer by layer to obtain Fig. (3e). In terms of the tensor elements, these TR-symmetric tensors are block-diagonal in a TR-symmetric basis. We now explain how to build TR-symmetric bases as we coarse grain the lattice via MERA.

For a MERA, or any other tensor network, to have a Z_2 symmetry, we require the tensors (w and u) to preserve the Z_2 symmetry; that is,

$$T_{i_1 i_2 \dots i_M} = 0, \text{ if } Z(i_1)Z(i_2) \dots Z(i_M) \neq 1; \quad (7)$$

where $Z(i_k) = \pm 1$, and the sign is $+$ ($-$) if the state labeled by i_k is Z_2 symmetric even(odd). To transform the basis into a Z_2 symmetric basis in the upper layers, we treat a tensor as an operator on a state by defining the *in*- and *out*-directions. The tensor is symmetric if the *in*- and *out*-states belong to the same symmetry sector (Fig. (4c)). To construct a Z_2 symmetric MERA, we first start from the physical layer and go up (Fig. 1). We go *in* the tensor from below and go *out* from the top. We first encounter the disentangler u , and the in-state is a linear combination of two physical sites. The symmetry of a combined state obeys the fusion rules:

$$\begin{aligned} (+) \otimes (+) &\rightarrow (+), \quad (-) \otimes (-) \rightarrow (+) \\ (+) \otimes (-) &\rightarrow (-), \quad (-) \otimes (+) \rightarrow (-), \end{aligned} \quad (8)$$

that is, if two sites are both in a Z_2 -symmetry even state, the combined state is Z_2 -symmetry even, etc. Recall that the operation of u can be regarded as a unitary transformation of

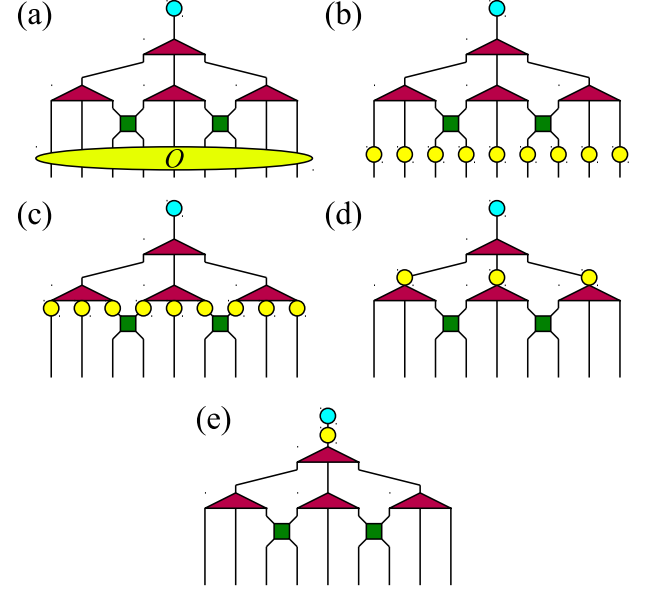


FIG. 3. (Color online) Commuting a TR symmetric MERA with TR operators (yellow circles). We want the operator in (a) to "jump" to the top as in (e). By enforcing all the w 's and u 's to be TR symmetric, we can break the TR operator into a product of local operators as shown in (b). Therefore, each operator can commute with the tensors locally, and we can *lift* the operators to the top of MERA through steps shown in (c)-(e).

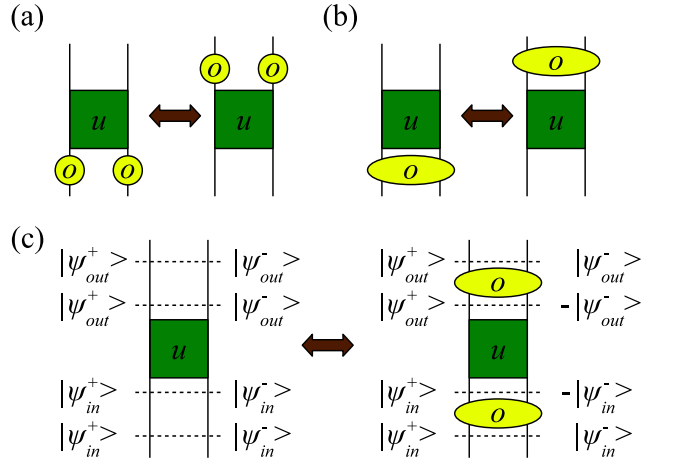


FIG. 4. (Color online) (a) Commuting two local TR operators with a disentangler u . (b) A global TR operator is constructed by grouping two local TR operators. (c) Applying another global TR operator at the bottom, in the diagram at the left, the operator becomes an identity while at the right, there are two TR operators above and below u . (Left) For a TR symmetric u , the in-state and out-state should be in the same symmetry sector. (Right) Application of the TR operator transforms the wave function as $|\psi_{in}^\pm\rangle \rightarrow \pm|\psi_{in}^\pm\rangle$. After the action of u , the states are still TR symmetric. Finally, after the second TR operator, we obtain the same out-states as those at the left.

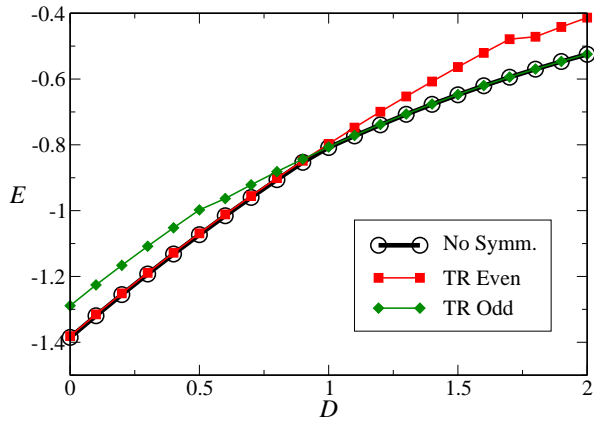


FIG. 5. (Color online) Lowest energy states obtained by MERA with (green diamond and red square) or without (black circle) imposing the time-reversal symmetry for $N = 9$, $\chi = 12$ ($\chi_{\text{even}} = \chi_{\text{odd}} = \chi/2$).

the wave function in the original basis; therefore, if u preserves the symmetry, the tensor elements of u corresponding to a transform from the in-states to the out-states in different symmetry sectors must be zero, which is exactly Eq. (7). Next comes an isometry w which coarse-grains three sites into one. If there is no truncation, we can regard w as a unitary transformation of the basis; i. e., the elements of w should give us information about how the new basis is formed by a linear combination of the incoming basis. To keep the outgoing basis Z_2 symmetric, we have to make sure that we do not mix bases belonging to different symmetry sectors. We perform truncations on the resulting Z_2 symmetry even and odd basis states independently. This process is repeated layer by layer to construct the Z_2 -symmetric MERA.

In practice, we initiate the tensors obeying the unitary constraints Eqs. (2) and (3), together with Eq. (7). During the SVD updates, the first two conditions are automatically satisfied,¹⁷ and the Z_2 symmetry is also satisfied because the environment satisfies Eq. (7), as it is formed by Z_2 -symmetric tensors. Therefore, in the symmetric basis (of the total in and out states), the environment tensor should be block-diagonal. Therefore we can perform the SVD block by block, and the updated tensor will also preserve the symmetry. For the same reason, the Hamiltonian at each layer will also be symmetric since the ascending operator is again obtained by contracting symmetric tensors. Finally, the top Hamiltonian is also block-diagonal. We can diagonalize the block for a specific symmetry sector to find the ground state.

To benchmark the algorithm, we show the ground states obtained by the TR symmetric MERA in the TR even and odd sectors, and compare it with the results from the non-symmetric MERA algorithm in Fig. 5. We show the results for an $N = 9$ chain with $\chi = 12$ ($\chi_{\text{even}} = \chi_{\text{odd}} = \chi/2$). The small system size is chosen such that the energy splitting between the states in different symmetry sectors is large deep inside the phase. For large D , the ground state is a product state $|0\rangle^{\otimes N}$. Under TR, $|0\rangle \rightarrow -|0\rangle$, and the ground state is TR odd. For small D , the ground state is the AKLT state,

which is TR even.⁸ This is a clear level crossing close to $D = 1$, indicating a phase transition.

Before moving to the next subsection, we would like to discuss how a Z_2 symmetric MERA can simplify the calculations by *removing* the Z_2 operator (denoted as O_{Z_2}) in the calculation. Consider a Z_2 operator $(O_{Z_2})_{i'_1}^{i_1}$ that operates on bond i'_1 of a symmetric disentangler $u_{i_3 i_4}^{i'_1 i_2}$. Assuming that the bond i'_1 is Z_2 symmetry even for $i'_1 = 1, 2, \dots, \chi_{\text{even}}$ and odd for the rest $\chi_{\text{odd}} = \chi - \chi_{\text{even}}$. The tensor element with i'_1 index for Z_2 symmetry even will not change, while the odd ones are multiplied by -1 after the application of O_{Z_2} . In our example, a TR operator operates on a TR symmetry even basis does nothing, while the operation change the sign of the state if the state is TR symmetry odd. That is, in a Z_2 symmetric basis:

$$(O_{Z_2})_{i'}^{i_1} = \delta_{i i'} Z(i). \quad (9)$$

Therefore, for a general Z_2 symmetric tensor T , we have:

$$\begin{aligned} (O_{Z_2})_{i'_1}^{i_1} \cdots (O_{Z_2})_{i'_M}^{i_M} T_{i'_1 \dots i'_M i_{k+1} \dots i_M} \\ = Z(i_1) \cdots Z(i_k) T_{i_1 \dots i_M}, \quad k \leq M \end{aligned} \quad (10)$$

Now if $k = M$ in Eq. (10), combining with Eq. (7), we have:

$$\begin{aligned} (O_{Z_2})_{i'_1}^{i_1} \cdots (O_{Z_2})_{i'_M}^{i_M} T_{i'_1 \dots i'_M} \\ = Z(i_1) \cdots Z(i_M) T_{i_1 \dots i_M} = T_{i_1 \dots i_M} \end{aligned} \quad (11)$$

since $T_{i_1 \dots i_M} \neq 0$ only if $Z(i_1) \cdots Z(i_M) = 1$. Therefore, if we operate O_{Z_2} on all the bonds of a Z_2 -symmetric tensor, the operations cancels each other. In addition, since $(O_{Z_2})^2 = \mathbb{I}$, we have (see Fig. 6):

$$\begin{aligned} (O_{Z_2})_{i'_1}^{i_1} \cdots (O_{Z_2})_{i'_k}^{i_k} T_{i'_1 \dots i'_k i_{k+1} \dots i_M} \\ = (O_{Z_2})_{i'_{k+1}}^{i_{k+1}} \cdots (O_{Z_2})_{i'_M}^{i_M} T_{i_1 \dots i_k i'_{k+1} \dots i'_M} \end{aligned} \quad (12)$$

This is essentially the *jump move* described in Ref. 22. We can move the symmetry operators to the boundary of the causal cone, and maintain the simple causal cone structure of a multi-site correlator in the calculation of these string-order parameters.

C. Inversion symmetric MERA

Incorporating inversion symmetry into MERA is non-trivial since the spatial inversion is defined *globally*. On the other hand, the tensors are *local* in the sense that they are only connected to part of the network. To perform a global inversion with local tensors requires special care. Figure 7 shows an example of how to geometrically invert a state composed of the product of two w 's. We first swap the top bonds for each tensor, and then invert each w about its own central bond. Hence, we can obtain a global inverted state by locally invert the tensors one-by-one geometrically. To understand how this geometrical operation can be translated into local tensor operations, we need to construct inversion symmetric

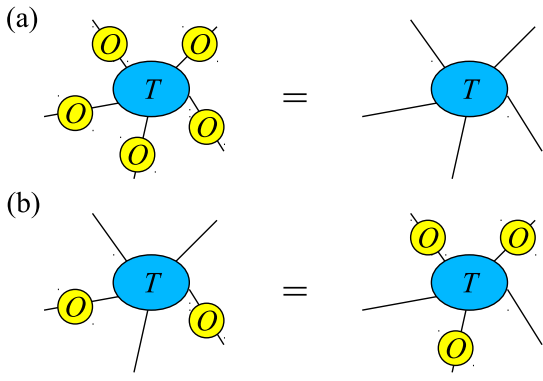


FIG. 6. (Color online) Diagrammatic representations of (a) Eq. (11) and (b) Eq. (12). T is a general symmetric tensor, and O is a Z_2 symmetry operator. The result of symmetry operations on some bonds of a symmetric tensor is the equivalent to the case where the operators operate on all the other bonds.

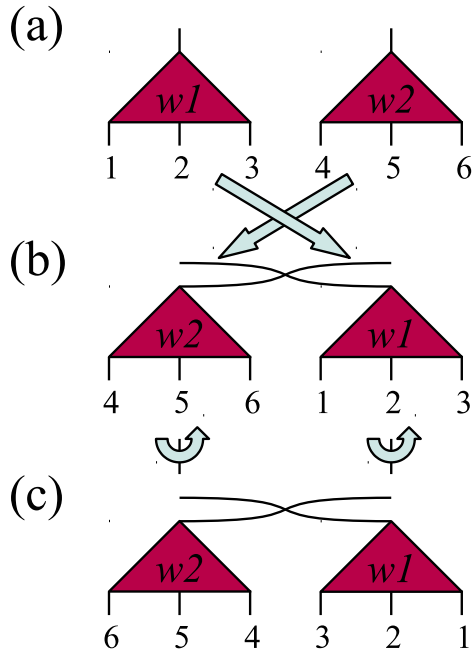


FIG. 7. (Color online) Geometrically, it takes two steps to invert the state composed of the product of two w 's (a). First, we swap the position of the w 's to obtain (b). Then we invert the w 's about their own central bonds to obtain (c). Finally, six sites are inverted.

basis by symmetrize or anti-symmetrize the original incoming and outgoing basis according to the fusion rules (see Appendix A). When the in- and out-basis are both transformed into the global inversion symmetric basis, an inversion symmetric tensor is block-diagonal. This is an analogy of Eq. (7) for inversion. In this case, the inverted state will be either the state itself (inversion even) or gains a minus sign (inversion odd).

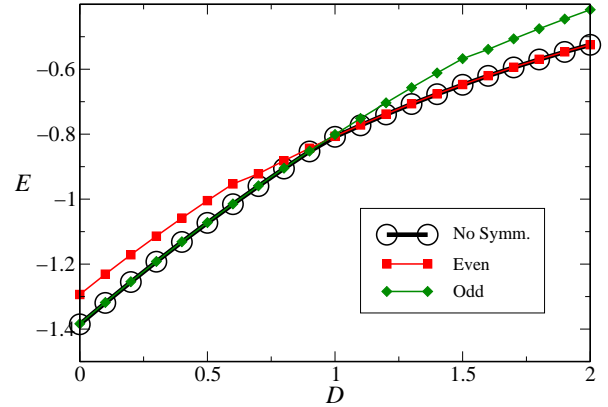


FIG. 8. (Color online) Lowest energy states obtained by MERA with (green diamond and red square) or without (black circle) imposing the inversion symmetry for $N = 9$, $\chi = 12$ ($\chi_{\text{even}} = \chi_{\text{odd}} = \chi/2$).

Figure 8 shows the result for an $N = 9$ chain with $\chi = 12$ ($\chi_{\text{even}} = \chi_{\text{odd}} = \chi/2$). The AKLT phase is known to be inversion odd for a periodic chain with odd number of sites⁸, and the large- D phase is inversion even. A level crossing near $D = 1$ indicates a topological phase transition from the topologically nontrivial Haldane phase to the topologically trivial large- D phase.

Before ending this subsection, we would like to discuss how one can simplify calculations in an inversion symmetric MERA by removing the inversion symmetry operator. This is more difficult than in the Z_2 -symmetry case, since the inversion operator can not be decomposed into local operators acting only on a single bond. Here, we present an analogy between the inversion of symmetric tensors and the geometrical inversion, called the *brick-and-rope* representation, to help us construct the necessary symmetry operations for inversion symmetric tensors.

Imagine one constructs a real-life MERA tensor network with *bricks*, representing tensors, and *ropes*, representing bonds (Fig. 9(a)). To obtain the inverted state, one needs only to rotate the whole structure by 180° (Fig. 9(b)). After the rotation, the structure would look very similar to the original except two crucial differences: the bricks are now turned to their *backsides*, and the top rope is *twisted*. Intuitively, given an inversion symmetric tensor, it is natural to argue that due to the inversion symmetry, the “backside” of the tensor should be the same as the tensor itself. Also, since the inverted MERA tensor network should represent the inversion of a state, a “twisted rope” would thus represent an inverted state. In the following, we will discuss how these physical intuitions can be realized using local tensor operations.

First, define a twisted *rope* (bond) as an inverted state. Note that in this definition, if the rope is twisted twice, it is equivalent to an untwisted rope since inverting a state twice will not change the state. Also at the physical layer, a twisted rope is equivalent to an untwisted rope since the inverted state corresponds to the state itself. For each bond, there are two types of basis states: symmetric states, denoted by $|S\rangle$, and anti-symmetric states, $|A\rangle$. When the bond is twisted, the basis

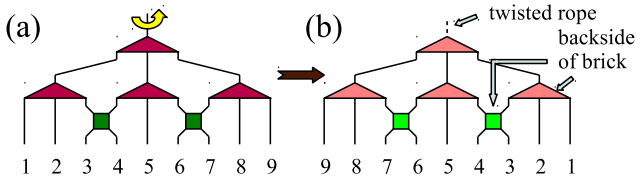


FIG. 9. (Color online) A real-life nine-site open boundary MERA constructed by *bricks*, representing tensors, and *ropes*, representing bonds. (a) is the original structure. We can easily invert the structure by rotating the whole structure about the central rope by 180° . The top rope is twisted, represented by dashed lines, and all the bricks turn to their backside, represented by a lighter color.

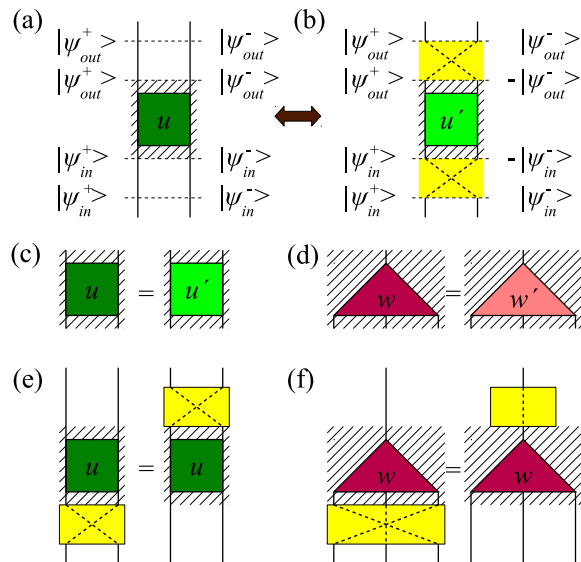


FIG. 10. (Color online) (a) Operating u on an inversion (anti-)symmetric state. (b) Rotating u to obtain its backside, with bonds swapped and twisted while holding the open ends of the bonds fixed. After the rotation, the originally inversion (anti-)symmetric state becomes (minus) itself, and the result after the u' operation is also (minus) itself. (c) u and u' are equal since the operation of u and u' is the same. (Shaded area is to make it clear that what we mean by u' does not include the dashed bonds.) It's the same for w as shown in (d). We further treat the yellow area (containing swapped and twisted bonds) as a local inversion operator. In analogy of Fig. 6, we obtain the jump rules for inversion symmetric MERA as shown in (e) and (f).

states would become $|S\rangle$ and $-|A\rangle$. Now, given an arbitrary u (Fig. 10(a)), we can obtain the inverted u by rotating the tensor while fixing the four external bonds (Fig. 10(b)). Therefore, operating u on a state $|\psi_{in}\rangle$ is equivalent to taking the following sequence: (1) Invert the incoming state $|\psi_{in}^\pm\rangle$. Note the bonds are also twisted, thus the basis states are inverted (Fig. 9). (2) Operate u' on the inverted state, and (3) invert the outgoing state $|\psi_{out}^\pm\rangle$. Now if the tensor is inversion symmetric, it preserves the symmetry property of the incoming state:

$$|\psi_{out}^\pm\rangle = u|\psi_{in}^\pm\rangle \quad (13)$$

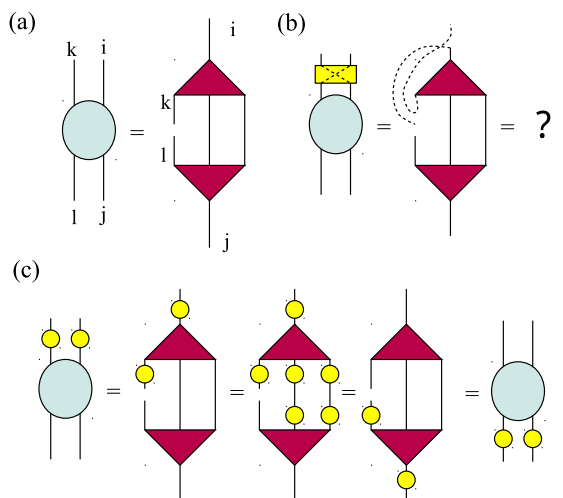


FIG. 11. (Color online) (a) Contraction of two bonds between inversion symmetric w and w^\dagger . (b) The resulting tensor is generally not inversion symmetric. (c) For internal symmetries, the resulting tensor is always symmetric.

During step (1), inverting the incoming symmetric state $|\psi_{in}^\pm\rangle$ gives $\pm|\psi_{in}^\pm\rangle$. Since the final outgoing state is still $|\psi_{out}^\pm\rangle$, so the state before the final inversion in step (3) should be $\pm|\psi_{out}^\pm\rangle$ (Fig. 10(b)). Combining these two equations, we get:

$$u'(\pm|\psi_{in}^\pm\rangle) = \pm|\psi_{out}^\pm\rangle \quad (14)$$

Comparing Eqs. (13) and (14), finally we have (Fig. 10(c)),

$$u = u', \quad (15)$$

which is exactly an inversion symmetric tensor. It is easy to show that the w 's also have this property; therefore, our brick-and-rope representation is self-consistent.

We can treat Fig. 10(e) and (f) as the jump rules for inversion symmetric tensors. The power of this representation can be shown in Fig. 9. We can either use the jump rules layer by layer to obtain Fig. 9(b), or we can simply geometrically invert the whole structure with the above interpretation for a twisted rope. The final result is the same but the whole process becomes much simpler, and it helps us move the inversion operator to the boundary of causal cone.

Finally, we want to emphasize one key difference between the global inversion symmetry and other internal symmetries. At the first glance, the jumps rules Figs. 10(e), and (f) looks similar to Figs. 6(a), and (b). However, taking a closer look, we find that the inversion operator can only jump between *fixed* in- and out-bonds. On the other hand, for any internal symmetry, we have the freedom to choose which bonds are designated as *in* and *out*. In the tensor contraction process, we normally contract two tensors at one time, so the operation generally produces some intermediate tensors. For an internal symmetry, these intermediate tensors are all symmetric.

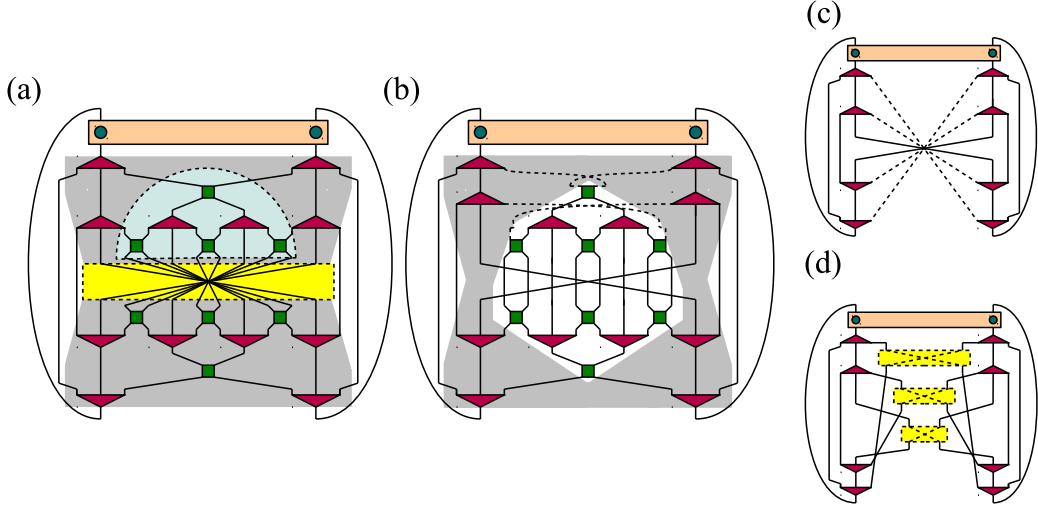


FIG. 12. (Color online) Reduction of the causal cone for an inversion symmetric string-order parameter. (a) shows the original diagram with ten inverted physical sites, and the shaded area is the original causal cone. (b) We invert the blue area (semi-circle) using the brick-and-rope representation. By doing so, the causal cone is much simplified. By contracting the tensors outside the causal cone, we obtain (c). In the sense of [Fig. 11](#), the tensors are lifted to the boundary of the (new) causal cone as shown in (d).

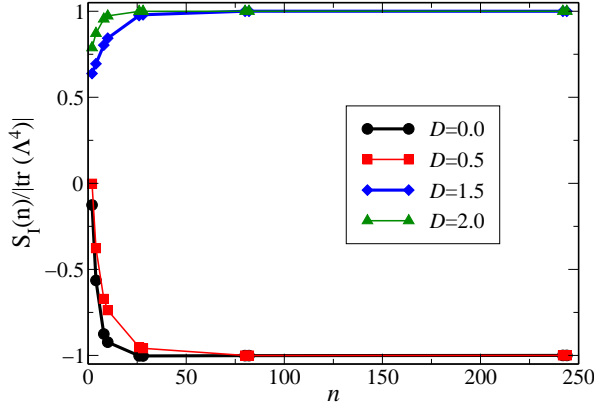


FIG. 13. (Color online) Inversion symmetric string-order parameter for $N = 486$ and $\chi = 12$ ($\chi_{\text{even}} = \chi_{\text{odd}} = \chi/2$).

However, for the inversion symmetry, only the *final* tensor is inversion symmetric. For example, in Fig. 11(a), we contract two bonds between two tensors w and w^\dagger , which is a typical process in MERA. The resulting tensor (Fig. 11(b)) for inversion symmetric w and w^\dagger is in general not inversion symmetric, while for internal symmetries, the intermediate tensor is still symmetric (Fig. 11(c)). On the other hand, although the intermediate tensors are not inversion symmetric, the final tensor will be symmetric if the full diagram is inversion symmetric. In fact, most of the diagrams in MERA are not inversion symmetric; e.g., two-thirds of the environment diagrams are not inversion symmetric.¹⁷ However, linear combination of these diagrams is inversion symmetric. In practice, this indicates that one can not use the inversion symmetry to reduce the computational cost as in the Z_2 case.

IV. DETECTING SYMMETRY PROTECTED TOPOLOGICAL PHASES WITH MERA

In Ref. 11, Turner and Pollmann proposed nonlocal string-order parameters to detect the topological phases protected by inversion and time-reversal symmetry. Although these order parameters are originally constructed in the iMPS formalism, direct calculation of these parameter by other methods should give the same results. In MERA, the calculation of these order parameters (Figs. 12 and 14) is generally much more involved than that of a two or three-site correlator. Using the symmetric MERA discussed above, we can apply the jump rules (Figs. 6 and 10) to *lift* the symmetry operators and the final causal cone has the same structure as that for a multi-site correlator, and the computation is greatly simplified.

A. String order in the presence of inversion symmetry

The order parameter for the inversion symmetry can be defined as the overlap of an infinite chain with a reverted segment,

$$S_I(n) = \langle \psi | I_{1,n} | \psi \rangle, \quad (16)$$

where $I_{1,n}$ is the inversion of the site 1 to n part of the chain. The limit as $n \rightarrow \infty$ is¹¹

$$\lim_{n \rightarrow \infty} S_I(n) = \pm \text{Tr}(\Lambda^4), \quad (17)$$

where the diagonal matrix Λ contains the Schmidt values λ_α of Schmidt decomposition of the ground state wave function,

$$|\psi\rangle = \sum_\alpha \lambda_\alpha |L_\alpha\rangle |R_\alpha\rangle, \quad (18)$$

where $|L_\alpha\rangle$ and $|R_\alpha\rangle$ are orthonormal basis vectors of the left and right partitions, respectively. For a topologically trivial state, the sign of $S_I(n)$ is positive, while for a topological nontrivial state, the sign is negative.¹¹

Figure 12(a) shows an example of a spin chain with ten inverted sites ($n = 10$). Using the brick-and-rope representation, we invert all the tensors in the blue half-circle to obtain Fig. 12(c), which can be easily calculated. If the number of inverted sites is equal to $3^k \pm 1$, $k \in \mathbb{N}$, as in this case, the boundary of the inversion operator is directly below the density matrix (Fig. 12(b)), the causal cone can be greatly simplified. For all other cases, the computation is more complicated.

For a periodic chain with even number of sites, the ground states in the Haldane and the large- D phases are both inversion symmetry even, and we can not use the level crossing method as in Sec. III C to distinguish these states. Figure 13 shows the results of the normalized string-order parameter $S_I(n)/|\text{tr}(\Lambda^4)|$ for several n 's up to $n = 244$ in a chain of size $N = 486$. In this case, we take $|\text{tr}(\Lambda^4)| = |S_I(244)|$ as it has reached the asymptotic value. It is clear that $S_I(n)/|\text{tr}(\Lambda^4)|$ reaches to ± 1 as n grows. For $D > 1$, the sign is positive, indicating a topologically trivial (large- D) phase. For $D < 1$, the sign is negative, indicating a topologically nontrivial (Haldane) phase.

B. String order parameters in the presence of time-reversal symmetry

For the time-reversal symmetry, the order parameter is defined as

$$S_{\text{TR}}(n) = d^n \langle \psi_2 | (|R_{1n}\rangle \langle R_{1n}|) \text{Swap}_{n+1,2n} | \psi_2 \rangle, \quad (19)$$

where

$$|\psi_2\rangle = |\psi\rangle \otimes |\psi\rangle$$

is two copies of the same wave function, and

$$|R_{1n}\rangle = \prod_{k=1}^n \left(\frac{1}{\sqrt{3}} \sum_{j_k} [e^{i\pi S^y}]_{j_k j'_k} |j_k\rangle \otimes |j'_k\rangle \right)$$

is the TR times the complex conjugation inserted from site 1 to site n . The $\text{Swap}_{n+1,2n}$ is the swap of site $n+1$ to site $2n$ between the two copies. As $n \rightarrow \infty$, $S_{\text{TR}}(n)$ reaches an asymptotic value,

$$\lim_{n \rightarrow \infty} S_{\text{TR}}(n) = \pm (\text{tr}(\Lambda^4))^3. \quad (20)$$

again, the sign is either positive or negative for a topologically trivial or non-trivial phase, respectively.

Figure 14 shows the diagrammatic representation of the order parameter S_{TR} for $n = 9$. It is more complicated as there are four wave functions with three domain walls. Again, here we choose a convenient setup of putting the domain walls at the sites of a three-site density matrix (Fig. 14(a)). By the application of jump rules for Z_2 symmetric tensors (Fig 6), we can lift the TR symmetry operators so that the causal cone is

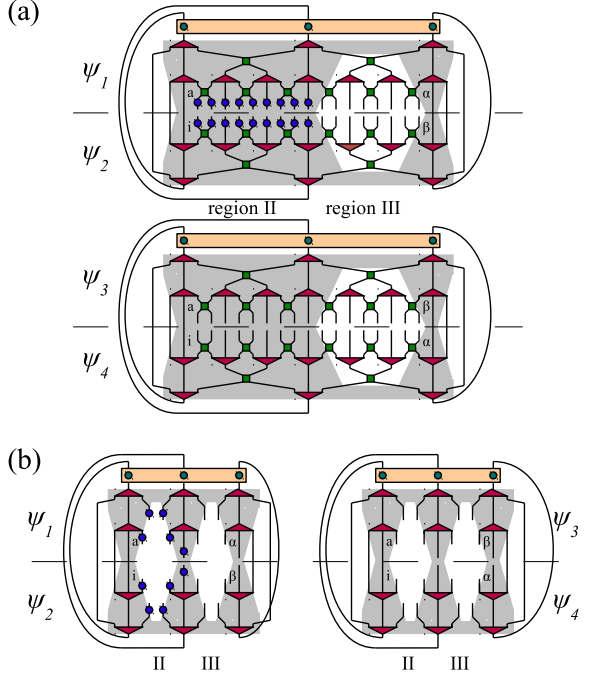


FIG. 14. (Color online) Diagrammatical representation of the $n = 9$ time-reversal string-order parameter in MERA. (a) The original diagram. The blue circles are the $e^{i\pi S^y}$ operators and the shaded area denotes the original causal cone. (b) The simplified diagram when the symmetry operators are lifted to the boundary of a new causal cone.

equivalent to that of a three-site correlator among sites at the domain walls. All the other tensors outside this causal cone are contracted to identity (Fig. 14(b)). For this choice of domain walls locations, the available $n = 3^k$, $k \in \mathbb{N}$.

For even number of sites, both the large- D and the Haldane phases are TR symmetry even, and we can not use level crossing to distinguish these phases. The string-order parameter, on the other hand, can still be used to distinguish these phases. Figure 16 shows $S_{\text{TR}}(n)$ for several n in a chain of $N = 486$. As n grows, $S_{\text{TR}}(n)$ reaches an asymptotic value. The sign of $S_{\text{TR}}(n)$ is either positive or negative for the Haldane phase or the large- D phase as expected.

V. SYMMETRY PROTECTED RENORMALIZATION GROUP FLOW

The extra dimension of MERA provides information about the RG flow during the coarse-graining transformation at different length scales. At the τ -th layer, we obtain an effective Hamiltonian H^τ and the coarse-grained wave function $|\psi^\tau\rangle$. If symmetric disentanglers and isometries are used in the entanglement renormalization process, we could obtain information about the symmetry-protected RG flow. In principle, one can take the symmetric disentanglers u and isometries w from the finite-size MERA for the buffer layers and construct a scale invariant MERA²¹ to obtain the fixed point ten-

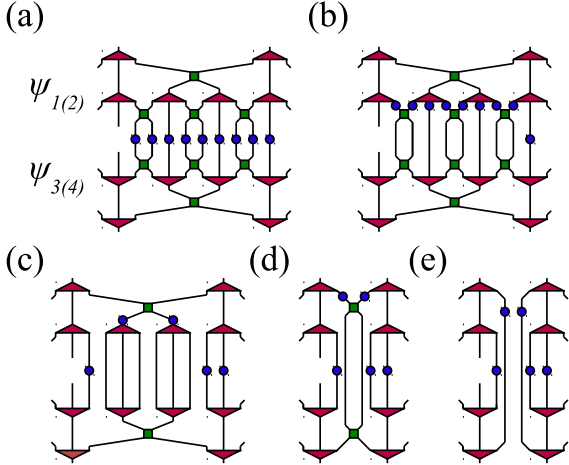


FIG. 15. (Color online) Reduction of the causal cone for $S_{TR}(n)$. (a) Contraction of ψ_1 and ψ_3 (or ψ_2 and ψ_4) in Region II. By using the jump rules, and Eqs. (2) and (3) successively, we obtain the intermediate diagrams (b),(c), and (d). Finally we obtain (e). For region III, the diagrams are exactly the same except there are no symmetry operators.

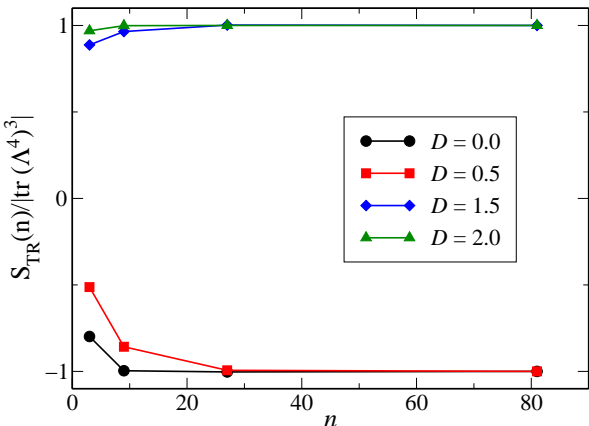


FIG. 16. (Color online) Time-reversal symmetric string-order parameters for $N = 486$ and $\chi = 12$ ($\chi_{\text{even}} = \chi_{\text{odd}} = \chi/2$).

sors for the SPT phases.^{15,25} Here we take a slightly different approach. We calculate the inversion symmetric order parameter at each layer as the system is coarse-grained. We expect the state will flow to either the AKLT state for $D < D_c$ or the large- D state for $D > D_c$ in the presence of symmetry. Therefore, the asymptotic value of the order parameter should flow to $-1/2$ for $D < D_c$ because the AKLT state has the Schmidt matrix¹¹

$$\Lambda_{\text{AKLT}} = \begin{pmatrix} \frac{1}{\sqrt{2}} & 0 \\ 0 & \frac{1}{\sqrt{2}} \end{pmatrix},$$

and $-\text{Tr}(\Lambda_{\text{AKLT}}^4) = -1/2$. On the other hand, for $D > D_c$, the state is expected to flow to a product state with $\Lambda_{\text{prod}} = 1$, and $\text{Tr}(\Lambda_{\text{prod}}^4) = 1$. Figure 17 shows the order parameter for the inversion symmetry, $S_I(n)$, at different length scales

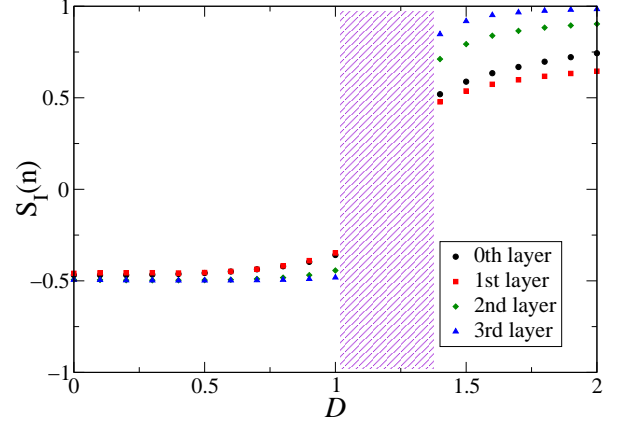


FIG. 17. (Color online) Order parameter for the inversion symmetry $S_I(n)$ at different length scales for a spin chain with $N = 1458$ and $\chi = 12$ ($\chi_{\text{even}} = \chi_{\text{odd}} = \chi/2$). The number of inverted sites for each layer is $n = 730, 244, 82$, and 28 , respectively. Shaded area indicates where $S_I(n)$ fails to reach asymptotic.

with $N = 1458$ and $\chi = 12$ ($\chi_{\text{even}} = \chi_{\text{odd}} = \chi/2$). The number of inverted sites for each layer is $n = 730, 244, 82$, and 28 , respectively. As we proceed the coarse-graining process from the physical (0th) layer to higher layers, we observe that for $D \lesssim 1$, the order parameter flows to the asymptotic value $-1/2$ as expected, and flows to 1 for large D . Notice in the regime of $D \gtrsim 1$, the flow to the product state is much slower, indicating the ground state is far away from the fixed point, and it requires more RG steps (or larger χ) to reach the asymptotic value 1. This also explains why $S_I(n)$ fails to reach the asymptotic value for $1 \lesssim D < 1.4$ (shaded area in Fig. 17).

VI. CONCLUSION

Global symmetries have been used extensively in MERA algorithms to reduce computation efforts, and to access different quantum number sectors.^{14,26,27} In this paper, we demonstrate how to use symmetric tensors in MERA to study the SPT phase for a given symmetric Hamiltonian.¹⁵ We have proposed a brick-and-rope representation for an inversion symmetric MERA, which gives a simple geometrical interpretation for inversion symmetric tensors. Using the time-reversal and inversion symmetric MERA, we demonstrate that the Haldane phase in spin-1 chain is protected by these symmetries. Finally, by computing the inversion symmetric string-order parameter at different length scales, we show that entanglement renormalization with symmetric tensors indeed provides information about the symmetry-protected RG flow, and the system does flow to a RG fixed point corresponding to the SPT phase. With the current scheme, it is easy to extend to spin chains and ladders with higher integer spins. Also, it can also be generalized to study the fractionalization of quasi-particles (edge states) by implementing the projective representation of the global symmetry in the symmetric tensors.

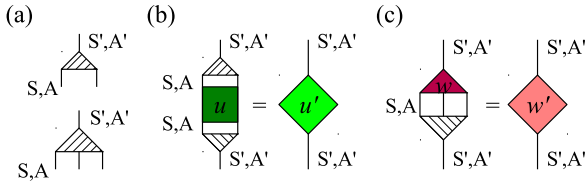


FIG. 18. (Color online) (a) The basis transformation tensors for u (top) and w (bottom), which transforms the original τ th-layer symmetric basis (S, A) into a $(\tau + 1)$ th-layer symmetric basis (S', A') . Operating these tensors on (b) u (green) and (c) w (red) makes them block-diagonal in the symmetric basis (S', A') .

ACKNOWLEDGMENTS

We thank G. Vidal and F. Pollmann for useful discussions. This work is partially supported by NSC in Taiwan through Grant No. 100-2112-M-002-013-MY3, 100-2923-M-004-002 -MY3- and by NTU Grant numbers 101R891004. Travel support from NCTS in Taiwan is also acknowledged.

Appendix A: Fusion rules for inversion symmetry

In this appendix, we present an example of the inversion fusion rules for u and w in MERA. As in the Z_2 case, we need to construct an inversion symmetric basis at each layer

of MERA. For simplicity, we take $S = 1/2$ as an example. At each physical site, there are two physical degrees of freedom, denoted by $|\uparrow\rangle$ and $|\downarrow\rangle$. At the physical (0th) layer, the fusion rules for u and w are given in Tabs. I and II. In terms of these basis states, u and w are block-diagonal (Fig. 18). At the first layer, for the illustration purpose, we keep only one symmetric state, denoted by S , and one anti-symmetric basis state, denoted by A . These states can be a linear combination of the original basis states. We symmetrize and anti-symmetrize these states to obtain a new basis for the $(\tau + 1)$ th-layer (Tabs. III and IV). Note that we have states that are by themselves anti-symmetric (e.g. SAS). Also, the symmetrized state for SSA is $(SSA - ASS)/\sqrt{2}$ while the anti-symmetrized state is $(SSA + ASS)/\sqrt{2}$. The reason for this can be easily observed from Fig. 7 that to invert a state, we not only swap the location of the bonds, but we twist these bonds as well, which will invert the tensors below. Notice that the fusion rules in Tabs. I and II only apply to the case where each site at the physical layer corresponds to one physical site. In this case, the inversion of single-site state at the physical layer is the state itself. If the sites at the physical layer are the composite of multiple physical sites, then the fusion rules in Tabs. III and IV should be used at the physical layer also. One can easily generalize the tables for a larger χ , where we have $S_i, i = 1, \dots, \chi_s$ and $A_i, i = 1, \dots, \chi_a$, with χ_s and χ_a being the bond dimensions for the symmetric and anti-symmetric sectors.

¹ X. G. Wen and Q. Niu, *Phys. Rev. B* **41**, 9377 (1990).
² X.-G. Wen, *Advances in Physics* **44**, 405 (1995).
³ X. Chen, Z.-C. Gu, and X.-G. Wen, *Phys. Rev. B* **82**, 155138 (2010).
⁴ X. Chen, Z.-C. Gu, and X.-G. Wen, *Phys. Rev. B* **83**, 035107 (2011).
⁵ Z.-C. Gu and X.-G. Wen, *Phys. Rev. B* **80**, 155131 (2009).
⁶ F. D. M. Haldane, *Phys. Rev. Lett.* **50**, 1153 (1983); F. Haldane, *Physics Letters A* **93**, 464 (1983).
⁷ F. Pollmann, A. M. Turner, E. Berg, and M. Oshikawa, *Phys. Rev. B* **81**, 064439 (2010).
⁸ I. Affleck, T. Kennedy, E. H. Lieb, and H. Tasaki, *Phys. Rev. Lett.* **59**, 799 (1987).
⁹ M. den Nijs and K. Rommelse, *Phys. Rev. B* **40**, 4709 (1989).
¹⁰ T. Kennedy and H. Tasaki, *Phys. Rev. B* **45**, 304 (1992).
¹¹ F. Pollmann and A. M. Turner, *Phys. Rev. B* **86**, 125441 (2012).
¹² J. Haegeman, D. Pérez-García, I. Cirac, and N. Schuch, *Phys. Rev. Lett.* **109**, 050402 (2012).
¹³ N. Schuch, D. Pérez-García, and I. Cirac, *Phys. Rev. B* **84**, 165139 (2011).
¹⁴ S. Singh, R. N. C. Pfeifer, and G. Vidal, *Phys. Rev. A* **82**, 050301 (2010).
¹⁵ S. Singh and G. Vidal, (2013), arxiv:1303.6716.
¹⁶ G. Vidal, *Phys. Rev. Lett.* **99**, 220405 (2007).
¹⁷ G. Evenbly and G. Vidal, *Phys. Rev. B* **79**, 144108 (2009).
¹⁸ G. Evenbly and G. Vidal, *Phys. Rev. Lett.* **102**, 180406 (2009).
¹⁹ G. Evenbly and G. Vidal, *Phys. Rev. Lett.* **104**, 187203 (2010).
²⁰ G. Evenbly and G. Vidal, *Phys. Rev. B* **81**, 235102 (2010).
²¹ R. N. C. Pfeifer, G. Evenbly, and G. Vidal, *Phys. Rev. A* **79**, 040301 (2009).
²² P. Corboz and G. Vidal, *Phys. Rev. B* **80**, 165129 (2009).
²³ G. Evenbly and G. Vidal, Unpublished.
²⁴ S. Hu, B. Normand, X. Wang, and L. Yu, *Phys. Rev. B* **84**, 220402 (2011).
²⁵ C.-Y. Huang, X. Chen, and F.-L. Lin, (2013), arXiv:1303.4190.
²⁶ S. Singh, R. N. C. Pfeifer, and G. Vidal, *Phys. Rev. B* **83**, 115125 (2011).
²⁷ S. Singh and G. Vidal, *Phys. Rev. B* **86**, 195114 (2012).

TABLE I. Fusion rules for u at the physical layer

Original basis	Symmetrized(S)	Anti-symmetrized(A)
$\begin{array}{c} \uparrow\uparrow \\ \uparrow\downarrow, \downarrow\uparrow \\ \downarrow\downarrow \end{array}$	$\begin{array}{c} \uparrow\uparrow \\ (\uparrow\downarrow + \downarrow\uparrow)/\sqrt{2} \\ \downarrow\downarrow \end{array}$	$\begin{array}{c} - \\ (\uparrow\downarrow - \downarrow\uparrow)/\sqrt{2} \\ - \end{array}$

TABLE II. Fusion rules for w at the physical layer

Original basis	Symmetrized(S)	Anti-symmetrized(A)
$\begin{array}{c} \uparrow\uparrow\uparrow \\ \uparrow\uparrow\downarrow, \downarrow\uparrow\uparrow \\ \uparrow\downarrow\uparrow \\ \uparrow\downarrow\downarrow, \downarrow\downarrow\uparrow \\ \downarrow\uparrow\downarrow \\ \downarrow\downarrow\downarrow \end{array}$	$\begin{array}{c} \uparrow\uparrow\uparrow \\ (\uparrow\uparrow\downarrow + \downarrow\uparrow\uparrow)/\sqrt{2} \\ \uparrow\downarrow\uparrow \\ (\uparrow\downarrow\downarrow + \downarrow\downarrow\uparrow)/\sqrt{2} \\ \downarrow\uparrow\downarrow \\ \downarrow\downarrow\downarrow \end{array}$	$\begin{array}{c} - \\ (\uparrow\uparrow\downarrow - \downarrow\uparrow\uparrow)/\sqrt{2} \\ - \\ (\uparrow\downarrow\downarrow - \downarrow\downarrow\uparrow)/\sqrt{2} \\ - \\ - \end{array}$

TABLE III. Fusion rules for u at upper layers

Original basis	Symmetrized(S')	Anti-symmetrized(A')
$\begin{array}{c} SS \\ SA, AS \\ AA \end{array}$	$\begin{array}{c} SS \\ (SA - AS)/\sqrt{2} \\ AA \end{array}$	$\begin{array}{c} - \\ (SA + AS)/\sqrt{2} \\ - \end{array}$

TABLE IV. Fusion rules for w at upper layers

Original basis	Symmetrized(S')	Anti-symmetrized(A')
$\begin{array}{c} SSS \\ SSA, ASS \\ SAS \\ SAA, AAS \\ ASA \\ AAA \end{array}$	$\begin{array}{c} SSS \\ (SSA - ASS)/\sqrt{2} \\ - \\ (SAA + AAS)/\sqrt{2} \\ ASA \\ - \end{array}$	$\begin{array}{c} - \\ (SSA + ASS)/\sqrt{2} \\ SAS \\ (SAA - AAS)/\sqrt{2} \\ - \\ AAA \end{array}$